Load Shedding and Restoration for Intentional Island with Renewable Distributed Generation

Jian Xu, *Senior Member*, *IEEE*, Boyu Xie, Siyang Liao, *Member*, *IEEE*, Zhiyong Yuan, Deping Ke, Yuanzhang Sun, *Senior Member*, *IEEE*, Xiong Li, and Xiaotao Peng, *Member*, *IEEE*

***Abstract*—Due to the high penetration of renewable distributed generation (RDG), many issues have become conspicuous during the intentional island operation such as the power mismatch of load shedding during the transition process and the power imbalance during the restoration process. In this paper, a phase measurement unit (PMU) based online load shedding strategy and a conservation voltage reduction (CVR) based multi-period restoration strategy are proposed for the intentional island with RDG. The proposed load shedding strategy, which is driven by the blackout event, consists of the load shedding optimization and correction table. Before the occurrence of the large-scale blackout, the load shedding optimization is solved periodically to obtain the optimal load shedding plan, which meets the dynamic and steady constraints. When the blackout occurs, the correction table updated in real time based on the PMU data is used to modify the load shedding plan to eliminate the power mismatch caused by the fluctuation of RDG. After the system transits to the intentional island seamlessly, multi-period restoration plans are generated to optimize the restoration performance while maintaining power balance until the main grid is repaired. Besides, CVR technology is implemented to restore more loads by regulating load demand. The proposed load shedding optimization and restoration optimization are linearized to mixed-integer quadratic constraint programming (MIQCP) models. The effectiveness of the proposed strategies is verified with the modified IEEE 33-node system on the real-time digital simulation (RTDS) platform.**

***Index Terms*—Intentional island, renewable distributed generation (RDG), load shedding, restoration, phase measurement unit (PMU), conservation voltage reduction (CVR).**

I. Introduction

DURING the past decades, the scale of power system expands rapidly due to the economic development and urban expansion. The complex power system provides more efficient energy, but makes reliability a challenging task, leading to more and more blackouts [1]. For example, dozens of large-scale blackouts occurred in the first half of 2019 such as in Venezuela and Britain, resulting in a significant loss of billions of dollars. The power supply to critical loads will be interrupted for a long time during blackout. Therefore, it is essential to improve the reliability of end-user oriented distribution system.

Fortunately, with the rapid development of distributed generation (DG) as well as advanced devices, the distribution system becomes active, controllable, and observable, which has the ability to form an intentional island to maintain the power supply during the external blackout. It is reported that cumulative installed distributed photovoltaic (PV) is projected to reach 60 GW by 2020 in China [2]. The low-cost remotely controllable switches and phase measurement unit (PMU) have also attracted widespread interests [3], [4]. In this context, the standard for intentional island operation was approved in 2009 [5]. The intentional island is similar to the islanded microgrid, but it is implemented in a wider range of medium-voltage distribution systems. As a special operation mode of smart distribution system, the intentional island can provide continuous power to critical users until the main grid is restored. However, the uncertainty of renewable distributed generation (RDG) has a great impact on the system operation, which must be considered to ensure the feasibility and reliability of the intentional island. According to the chronological order, the processes of the intentional island can be divided into transition, restoration, and reconnection processes. This paper mainly focuses on the first two processes.

When a blackout occurs, the massive power deficit caused by the interruption of the main grid will result in a rapid frequency drop, and the governors of dispatchable DGs may fail to maintain the stability of the intentional island with low inertia. Therefore, it is necessary to shed some non-critical loads to rebalance the system quickly to ensure the uninterrupted supply of critical loads.

Traditionally, the load shedding strategy generally responds to the changes of frequency and sheds a predefined load when the frequency falls below a certain threshold. Reference [6] designs an under-frequency load shedding plan for the Danish power system with high penetration of wind power. A semi-adaptive load shedding strategy is proposed

Manuscript received: September 30, 2019; accepted: October 26, 2020. Date of CrossCheck: October 26, 2020. Date of online publication: April 21, 2021.

This work was supported in part by the National Key R&D Program of China (No. 2017YFB0902900), the National Natural Science Foundation of China (No. 51707136), and the Natural Science Foundation of Hubei Province (No. 2018CFA080).

J. Xu, B. Xie, S. Liao (corresponding author), D. Ke, Y. Sun, X. Li, and X. Peng are with the School of Electrical Engineering and Automations, Wuhan University, Wuhan 430072, China (e-mail: xujian@whu.edu.cn; xieboyv@whu.edu.cn; liaosiyang@whu.edu.cn; kedeping@whu.edu.cn; yzsun@mail.tsinghua.edu.cn; lixiong2000@263.net; pengxiaotao@whu.edu.cn).

Z. Yuan is with the China Southern Power Grid Research Institute, China Southern Power Grid Company, Guangzhou 510663, China (e-mail: yuanzy@csg.cn).

DOI: 10.35833/MPCE.2019.000062

in [7], which employs both the frequency and rate of change of frequency (ROCOF) as the thresholds. Reference [8] proposes an adaptive load shedding scheme, where the number of loads to be shed is accurately estimated through the swing equation and ROCOF. In [9], a centralized adaptive load shedding method is designed, which uses the state estimator to determine the power of each bus in order to shed the load at the correct location. The droop characteristics of dispatchable DGs are considered in [10] when estimating the number of loads to be shed. In [11], the power flow tracing technology is utilized to determine the amount of load shedding of each bus; besides, the topology constraint is also taken into account. The conventional load shedding, semi-adaptive load shedding, and adaptive load shedding strategies are analyzed and compared in [12]. The above load shedding strategies are response-based load shedding (RLS) strategies, which respond to the frequency and ROCOF obtained by PMU. However, the estimation performance of ROCOF in the transient process is poor since PMU relies on the static signal model, which may result in a wrong load shedding [13]. Furthermore, the load shedding action of RLS is activated only when the frequency is below the threshold, and such a long delay may cause the system to collapse. Therefore, the event-based load shedding (ELS) strategy is proposed, which is activated by a specific trigger signal, such as the status of the breaker. For example, [14] proposes an ELS strategy for the microgrid islanding event. In [15], the amount and location of loads to be shed for the possible contingency are calculated periodically and stored in a look-up table.

Meanwhile, the cost of load shedding is high, and it is essential to optimize the load shedding plan to achieve the required seamless transition with the minimum load curtailment. Besides, the uncertainty of RDG should also be taken into account to ensure the feasibility of load shedding plan. A bi-level optimization is proposed in [16], which combines the preventive dispatch and the load shedding to achieve the minimum coordination cost. Reference [17] employs the Lagrange multipliers to optimize the load shedding locations. In [18], a stochastic load shedding optimization is proposed to maximize the economic performance, where the Markov decision model is utilized to solve the uncertainty of RDG. A robust ELS strategy with steady constraints is proposed in [19], which is periodically calculated to consider the uncertainty. Besides, some intelligent algorithms such as genetic algorithm [20], particle swarm optimization [21], heuristic strategy [22], and multi-agent system [23] are also utilized to solve the load shedding optimization. However, due to the nonlinear constraints and the binary variables, the load shedding optimization generally requires a long solution time. Besides, the power of PV fluctuates rapidly, and the ramp rate is up to 70%/min in the field [24]. The real-time power fluctuation may lead to a large power mismatch in load shedding plan, especially in the intentional island with low inertia but a high penetration of RDG, which cannot be ignored. However, few researchers have addressed the problem of online optimal load shedding with both steady and dynamic constraints, while considering the real-time power change of RDG.

The duration of the intentional island operation depends on the repair time of the main grid, which may take a few hours. However, the output of RDG and the demand of customers change significantly on a long time scale, which may cause the system to collapse when there is a large unbalanced power. Therefore, after the transition, the restoration strategy is desired to make full use of resources to maintain the power balance and optimize the restoration performance.

Many research works in recent years have focused on the restoration of distribution system [25]. For example, some intelligent algorithms such as heuristic strategy [26], multi-agent system [27], and genetic algorithm [28] are utilized to solve the restoration problem. However, these methods may not always ensure global optimal restoration plan, so mathematical programming has been widely used. For example, [29] proposes a two-stage single-period optimization model, where the graph theory and optimal power flow (OPF) technology are employed to find the optimal restoration plan with the maximum load recovery. In [30], a multi-period mixed-integer linear programming (MILP) is designed to dynamically adjust resources to maintain the system stability. In [31], the switches are categorized into six groups, and different switches are optimized at different stages to reduce the solution time. In [32], a complex mixed-integer nonlinear restoration problem is proposed and solved by the modified combinatorial Benders algorithm. A multi-time step restoration strategy is proposed in [33], which can optimize the control sequence of switches, DGs, and energy storage. In [34], the internal combustion engine vehicles are utilized as the backup energy source to restore the critical loads. The output of RDG is random, and its uncertainty has a great impact on the determination of the restoration plan. Therefore, in [35], the chance-constrained restoration optimization is proposed, where the PV output is represented by different scenarios. In [36], a robust mixed-integer optimization model is proposed, where the final restoration plan is related to the worst-case scenario. The latest forecasting of renewable generation is used as the input in [37], and the output of wind generators are represented by Markov states in [38] to reduce the DG curtailment and load shedding. However, previous works have focused only on the traditional control resources, i. e., the adjustment of DG output and load shedding, which ignores the continuous adjustment potential of load demand.

Load demand can be regulated flexibly, which is usually realized through the financial compensation of demand response (DR). However, the performance of DR depends on the response of the end-user [39], which is highly uncertain, especially in emergency circumstances. In practice, system operators can regulate the load demand independently based on conservation voltage reduction (CVR), which is a direct load control technology based on the fact that most loads are sensitive to the voltage [40]. The load demand can be regulated continuously by adjusting voltage within the statutory limits. Some applications of CVR have been investigated in energy saving [41] and peak demand reduction [42]. However, there is no research on the restoration of the intentional island based on CVR to increase the number of the restored customers.

Motivated by the challenges mentioned above, this paper proposes a PMU-based online load shedding strategy and a CVR-based multi-period restoration strategy for the intentional island with RDG. Besides, the modified IEEE 33-node system is employed to verify the effectiveness of the proposed strategies. The main contributions are as follows.

1) An online load shedding strategy is proposed based on the real-time PMU data. The existing strategy only updates the load shedding plan periodically, which may be invalid in the scenarios with rapid fluctuations of PV and loads. By combining the load shedding optimization with the correction table, the proposed load shedding strategy can obtain the optimal load shedding plan online and ensure the smooth transition of the intentional island with the minimum load shedding cost. Besides, the load shedding optimization, which meets dynamic and steady constraints, is linearized to a mixed-integer quadratic constraint programming (MIQCP).

2) Compared with previous restoration research works that focus on the optimization of DG output and load shedding, this paper exploits the continuous adjustment of load demand based on CVR during the restoration process. With limited DG capacity, the restoration performance can be further improved. Meanwhile, the restoration problem is formulated as multi-period optimization to adjust the restoration plans dynamically in order to adapt to the intermittence of PV output, which is also linearized to MIQCP. Besides, the impacts of the forecasting errors of PV output are also considered in the dynamic scenario.

The remainder of this paper is organized as follows. Section II describes the intentional island. The load shedding strategy and restoration strategy are introduced in Section III and Section IV, respectively. In Section V, the simplified methods for load shedding optimization and restoration optimization are presented. The case study is given in Section VI, whereas concluding remarks are given in Section VII.

II. Intentional Island

The intentional island discussed in this paper is a medium-voltage distribution system, which has only one transmission line connected to the main grid and is prone to large-scale blackouts. This system is widespread in the mountains of southern China. The substation is regarded as the point of common coupling (PCC) between the main grid and the intentional island. The status of the breaker at the PCC can be regarded as the indicator signal of the load shedding event, which is continuously monitored by the distributed management system (DMS). There are dispatchable DGs and RDGs in the intentional island. The output and terminal voltages of the dispatchable DGs can be controlled by DMS. The active power of PV depends on the solar irradiance and temperature, but the reactive power can be regulated to perform CVR. During the intentional island operation, the dispatchable DG with the largest capacity is the master DG that maintains the stability of the island, while other DGs are the slave ones with constant output. Most loads in the modern distribution system are equipped with remote units such as the distribution terminal unit (DTU) and smart switch [33], which enable the load to be remotely restored or shed. The framework of the proposed load shedding strategy and restoration strategy is shown in Fig. 1.

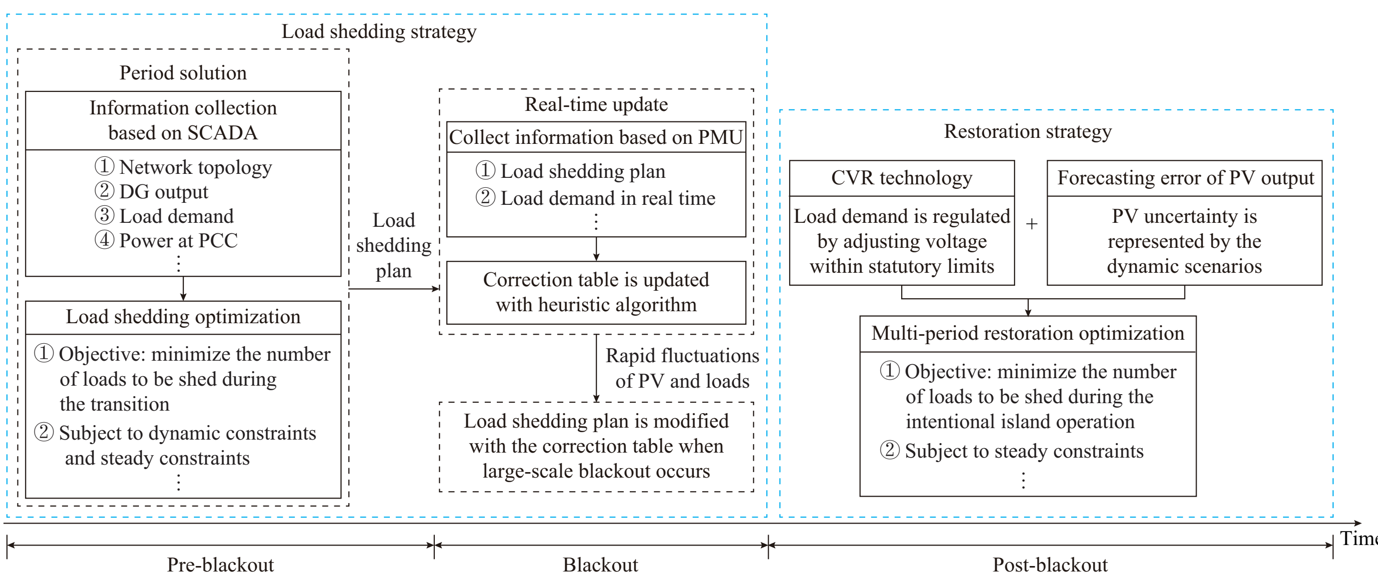

Fig. 1. Framework of proposed load shedding strategy and restoration strategy.

A. Load Shedding Strategy

The proposed load shedding strategy consists of the load shedding optimization and correction table. Firstly, before the blackout occurs, the load shedding optimization is solved periodically based on the snapshot of the system. The calculated load shedding plan meets various constraints with the minimum load shedding cost. Meanwhile, the correction table is updated in real time based on the PMU data with the heuristic algorithm. Then, once the DMS detects the occurrence of blackout event, the load shedding process is activated immediately. According to the power difference at PCC between the moments of blackout and optimization, i. e., ΔP^{PCC}, the correction table modifies the load shedding plan online to reduce the power mismatch caused by PV. For example, $\Delta P^{\mathrm{PCC}} > 0$ indicates that the DG output reduces or the load demand increases compared with that at the optimization moment. Therefore, in addition to the loads in the precalculated load shedding plan, some other non-critical loads need to be shed. The details about the load shedding strategy are presented in Section III.

B. Restoration Strategy

During the intentional island operation, due to the rapid fluctuation of PV, it is necessary to generate multi-period restoration plans to ensure the power balance and improve the restoration performance during each time period. For the proposed restoration strategy, in addition to the optimization of DG output, load shedding, and restoration, CVR is implemented through the volt/var control to regulate the load demand to restore more customers. Besides, the PV outputs are represented by dynamic scenarios to reduce the impacts of forecasting errors. Meanwhile, the multi-period restoration optimization is solved through the look-ahead method [30]. The look-ahead method solves the optimization repeatedly as time moves forward and obtains restoration plans over the optimization window, but only the plan for the next period is implemented in practice. The details about the restoration strategy are presented in Section IV.

III. Load Shedding Strategy

A. Load Shedding Optimization

The objective of load shedding optimization is to minimize the number of loads to be shed, which is expressed as:

$$\min \sum_{i \in I} c_i x_i \tag{1}$$

$$c_i = \rho_i + n_i \tag{2}$$

where c_i is the load weight; ρ_i is the priority factor; n_i is the customer factor; I is the set of loads; and the load status x_i is the decision variable, which is a binary variable, and $x_i = 1$ indicates that load i is to be shed.

According to the losses caused by blackouts, the priority of load is divided into three classes [43]. The first-class load is the very important load with the highest priority factor such as hospital; the second-class load is the important load such as shopping mall; and the third-class load has the lowest priority factor such as resident. In most existing studies, the load weight is only related to the load priority [15], [20]. In order to improve the reliability indices and reduce the customer complaints, the load weight is also related to the customer factor in this paper. Customer factor is the ratio of the number of customers of the load to the total number of customers with the same priority.

The system average interruption duration index (SAIDI) is one of the most critical reliability indices [44], which indicates the duration of interruption for the average customer and it is formulated as:

$$SAIDI = \sum_{k \in K} \sum_{i \in I} \frac{r_k N_{i,k}}{N_T} \tag{3}$$

where r_k is the duration time of blackout k; $N_{i,k}$ is the number of customers of load i affected by blackout k; K is the set of blackouts; and N_T is the total number of customers.

SAIDI plays an important role in the reliability assessment, and it is essential to reduce the SAIDI for both power utilities and customers. When facing load with the same priority, based on the customer factor, the optimization program can preferentially select the load with a small number of customers to be shed, thereby reducing the SAIDI as well as the customer complaints.

The constraints of the load shedding optimization include:

1) Dynamic Constraint

Since the large frequency drop may trigger the cascading event, the frequency deviation during the transition process should be limited by:

$$\Delta f \le \Delta f^{\max} \tag{4}$$

where Δf is the frequency deviation; and $\Delta f^{\max}$ is the frequency limit.

2) Steady Constraints

The operation of the intentional island should meet the power flow constraints. Besides, the power at PCC S^{PCC} should be limited to zero.

$$P_i - \mathrm{j}Q_i = \left(V_i\right)^* \sum_{j \in \Omega_i} Y_{ij} V_j \tag{5}$$

$$S^{\mathrm{PCC}} = 0 \tag{6}$$

where P_i and Q_i are the injected active and reactive power at node i, respectively; V_i and V_j are the voltage of node i and node j; Ω_i is the node set connected to node i; and Y_{ij} is the conductance between node i and node j.

Besides, the node voltage should be within the allowable ranges as shown in (7).

$$V^{\min} \le \left| V_i \right| \le V^{\max} \tag{7}$$

where $\left| V_i \right|$ is the voltage amplitude of node i; and $V^{\min}$ and $V^{\max}$ are the minimum and maximum limits of voltage, respectively.

The line current should also not exceed its allowable range.

$$I_l \le I^{\max} \tag{8}$$

where I_l is the line current; and $I^{\max}$ is the current limit.

3) DG Constraints

The output of dispatchable DG should be within the ramp limits process.

$$\Delta P_g^{\mathrm{dn,tr}} \le P_g^{\mathrm{DDG}} - P_g^{\mathrm{DDG,bef}} \le \Delta P_g^{\mathrm{up,tr}} \tag{9}$$

where $P_g^{\mathrm{DDG,bef}}$ and P_g^{DDG} are the active power of dispatchable DG g before and after the transition, respectively; and $\Delta P_g^{\mathrm{up,tr}}$ and $\Delta P_g^{\mathrm{dn,tr}}$ are the ramp-up and ramp-down active power of dispatchable DG g during the transition process, respectively.

The output of RDG should be unchanged during the transition.

$$P_g^{\mathrm{RDG}} = P_g^{\mathrm{RDG,bef}} \tag{10}$$

$$Q_g^{\mathrm{RDG}} = Q_g^{\mathrm{RDG,bef}} \tag{11}$$

where $P_g^{\mathrm{RDG,bef}}$, P_g^{RDG}, $Q_g^{\mathrm{RDG,bef}}$, and Q_g^{RDG} are the active and the reactive power of RDG g before and after the transition, respectively.

In addition, each DG should be within its rated capacity.

$$\left(P_g^{\mathrm{DG}}\right)^2+\left(Q_g^{\mathrm{DG}}\right)^2 \le \left(S_g^{\mathrm{DG}}\right)^2 \tag{12}$$

where S_g^{DG} is the rated capacity of DG g.

4) Load Constraints

The ZIP load model is utilized to represent the dependence of the load on voltage, which is formulated as:

$$P_i = x_i P_i^{\mathrm{N}}\left[Z_i^{\mathrm{P}}\left(V_i/V_i^{\mathrm{N}}\right)^2 + I_i^{\mathrm{P}}\left(V_i/V_i^{\mathrm{N}}\right)+P_i^{\mathrm{P}}\right] \tag{13}$$

$$Q_i = x_i Q_i^{\mathrm{N}}\left[Z_i^{\mathrm{Q}}\left(V_i/V_i^{\mathrm{N}}\right)^2 + I_i^{\mathrm{Q}}\left(V_i/V_i^{\mathrm{N}}\right)+P_i^{\mathrm{Q}}\right] \tag{14}$$

where P_i^{N} and Q_i^{N} are the rated active and reactive power of load at the rated voltage V_i^{N}, respectively; and Z_i^{P}, I_i^{P}, P_i^{P}, Z_i^{Q}, I_i^{Q}, and P_i^{Q} are the ZIP coefficients.

Meanwhile, it also should be noted that only the load equipped with the remote breaker can be shed, which is shown as:

$$x_i = \begin{cases} 0 & \text{load is not equipped with remote breaker} \\ & \text{or it is not to be shed} \\ 1 & \text{load is equipped with remote breaker} \\ & \text{and it is to be shed} \end{cases} \tag{15}$$

B. Correction Table

Due to the influence of dynamic constraints and the binary-continuous variables, the calculation burden of load shedding optimization is heavy. Even if the optimization model is solved periodically, there is still a power mismatch between the DG output and load demand in the load shedding plan when the fluctuation of PV is rapid. Therefore, in order to make a correct load shedding decision online, the correction table is proposed as an auxiliary tool for load shedding optimization. The power difference at PCC between the moments of blackout and optimization ΔP^{PCC} indicates the mismatch level of the load shedding plan, which can be reduced by additionally shedding or restoring loads. The input item of the correction table is ΔP^{PCC}, and the output item is the corrective load combination. By determining which condition the input satisfies, the output corresponding to this condition is quickly selected to modify the load shedding plan.

It should be noted that, compared with the load shedding optimization, the correction table is only providing a feasible correction scheme quickly, but may not be optimal. In order to ensure that the calculation results of the correction table are consistent with the load shedding optimization results, the load selection principles of the correction table are designed.

1) The load with lower priority should be shed preferentially and restored later.

2) For the same power deficit, the load with the same priority but with fewer customers should be shed preferentially and restored later.

The first principle is used to deal with the selection of loads with different priorities, and its role is the same as the priority factor in the load shedding optimization, ensuring that the load with higher priority is restored preferentially. The second principle is used to deal with the selection of loads with the same priority, and its role is the same as the customer factor. Based on the above principles, a heuristic algorithm that can quickly generate the correction table is proposed. There are only two scenarios in the correction table: additional load restoration ($\Delta P^{\mathrm{PCC}}>0$) and additional load shedding ($\Delta P^{\mathrm{PCC}}<0$). An example is given below to illustrate the generation process of the correction table in the case of additional load restoration with the heuristic algorithm, and the generation process of additional load shedding is similar.

Step 1: identify the set of loads to be shed and obtain their information. For example, according to the pre-calculated load shedding plan, loads L_1, L_2, and L_3 are to be shed when the blackout occurs. Their priority factors are $\rho_1=10$, $\rho_2=1$, and $\rho_3=1$, respectively. The number of their customers are $N_1=58$, $N_2=99$, and $N_3=59$, respectively, and their power demands are $P_1=50$ kW, $P_2=204$ kW, and $P_3=63$ kW, respectively.

Step 2: generate power segment points according to the combination of load demand. According to the load demand of L_1, L_2, and L_3, seven power segment points are generated: {50 kW, 63 kW, 113 kW, 204 kW, 254 kW, 267 kW, 317 kW}.

Step 3: generate power intervals according to the ascending order of power segment points. Arrange the segment points in ascending order, and generate seven power intervals, namely seven scenarios, including $\{S_1, 50\ \text{kW} \le \Delta P^{\mathrm{PCC}} < 63\ \text{kW}\}$, $\{S_2, 63\ \text{kW} \le \Delta P^{\mathrm{PCC}} < 113\ \text{kW}\}$, $\{S_3, 113\ \text{kW} \le \Delta P^{\mathrm{PCC}} < 204\ \text{kW}\}$, $\{S_4, 204\ \text{kW} \le \Delta P^{\mathrm{PCC}} < 254\ \text{kW}\}$, $\{S_5, 254\ \text{kW} \le \Delta P^{\mathrm{PCC}} < 267\ \text{kW}\}$, $\{S_6, 267\ \text{kW} \le \Delta P^{\mathrm{PCC}} < 317\ \text{kW}\}$, and $\{S_7, 317\ \text{kW} \le \Delta P^{\mathrm{PCC}}\}$.

Step 4: for each power interval, select appropriate loads according to the proposed principles to form a load combination. The total load demand in the load combination should be less than the lower limit of the power interval, and each combination should contain as many loads as possible. According to the proposed principles, for the loads with different priorities, the load with higher priority is selected preferentially. Then, for the loads with the same priority, the load with more customers is selected preferentially. Therefore, for $\{S_1, 50\ \text{kW} \le \Delta P^{\mathrm{PCC}} < 63\ \text{kW}\}$, L_1 is preferentially selected due to its high priority, and no other loads can be further selected due to the power limit. Thus, the load combination of S_1 is $\{L_1\}$. For $\{S_2, 63\ \text{kW} \le \Delta P^{\mathrm{PCC}} < 113\ \text{kW}\}$, due to the priority of L_1 is higher than L_3, the corresponding load combination is also $\{L_1\}$. For $\{S_3, 113\ \text{kW} \le \Delta P^{\mathrm{PCC}} < 204\ \text{kW}\}$, L_3 is also selected in addition to L_1, i. e., the load combination is $\{L_1, L_3\}$. For $\{S_4, 204\ \text{kW} \le \Delta P^{\mathrm{PCC}} < 254\ \text{kW}\}$, the load combination is also $\{L_1, L_3\}$ due to the power limit. For $\{S_5, 254\ \text{kW} \le \Delta P^{\mathrm{PCC}} < 267\ \text{kW}\}$, although L_2 and L_3 have the same priority, L_2 is selected preferentially because it has more customers, and the load combination is $\{L_1, L_2\}$. For $\{S_6, 267\ \text{kW} \le \Delta P^{\mathrm{PCC}} < 317\ \text{kW}\}$, no more load can be selected due to the power limit, and the load combination is also $\{L_1, L_2\}$. For $\{S_7, 317\ \text{kW} \le \Delta P^{\mathrm{PCC}}\}$, all loads are selected, and the load combination is $\{L_1, L_2, L_3\}$.

Step 5: generate the correction table. The condition of the correction table is that ΔP^{PCC} is within the power interval. The result is to restore all the loads in the load combination corresponding to the power interval. The example of correction table is generated, as shown in Table I.

TABLE I
EXAMPLE OF CORRECTION TABLE

Scenario	Power interval	Results of load shedding correction
S_1	$50\ \text{kW} \le \Delta P^{\text{PCC}} < 63\ \text{kW}$	Restore L_1
S_2	$63\ \text{kW} \le \Delta P^{\text{PCC}} < 113\ \text{kW}$	Restore L_1
S_3	$113\ \text{kW} \le \Delta P^{\text{PCC}} < 204\ \text{kW}$	Restore L_1, L_3
S_4	$204\ \text{kW} \le \Delta P^{\text{PCC}} < 254\ \text{kW}$	Restore L_1, L_3
S_5	$254\ \text{kW} \le \Delta P^{\text{PCC}} < 267\ \text{kW}$	Restore L_1, L_2
S_6	$267\ \text{kW} \le \Delta P^{\text{PCC}} < 317\ \text{kW}$	Restore L_1, L_2
S_7	$317\ \text{kW} \le \Delta P^{\text{PCC}}$	Restore L_1, L_2, L_3

It should be noted that as the number of loads N increases, the number of power intervals will increase to $2^N - 1$. In order to find a tradeoff between the optimality and the speed, the total number of power intervals for $\Delta P^{\text{PCC}} > 0$ and $\Delta P^{\text{PCC}} < 0$ is limited to 20 in this paper. The power intervals can be 20 equal intervals between the minimum and the maximum power segment points. Although the limited number of power intervals reduces the optimality, it improves the update speed and ensures the validity of correction table. Meanwhile, the number of power intervals can be changed flexibly according to the actual situation. The correction table can be updated within 3 s using the heuristic algorithm.

IV. RESTORATION STRATEGY

A. CVR

CVR is a load control technology based on the fact that most loads are sensitive to voltage. There have been extensive CVR tests around the world. The effect of CVR depends on the load composition, which is usually 0.3%-1% load reduction per 1% voltage reduction. The effect of CVR is quantified by the CVR factor, as shown in (16).

$$CVR_{\text{factor}} = \Delta P / \Delta V \tag{16}$$

where ΔV is the voltage reduction; and ΔP is the power deficit.

Different loads have different CVR factors. In general, the CVR factors of commercial, residential, municipal, and industrial loads are 0.99%, 0.76%, 0.76%, and 0.41%, respectively [40].

B. PV Uncertainty

The PV forecasting is the indispensable input for multi-period restoration optimization. In this paper, a dynamic scenario generation method and a scenario reduction method are utilized to reduce the impact of forecasting error [45]. Firstly, the continuous random variable is obtained according to the multivariate normal distribution, and then the cumulative probability of the continuous variable is calculated with the cumulative standard normal distribution function. Then, the dynamic scenario of PV is generated by the inverse function of empirical cumulative distribution in each forecasting bin. Then, the scenario reduction method based on the backward-reduction algorithm is utilized to reduce the number of scenarios. Compared with the static scenario, the dynamic scenario can reflect the time correlation of the PV output, which is more suitable for multi-period restoration optimization.

C. Restoration Optimization

The objective of restoration optimization is to minimize the number of loads to be shed over the optimization window. The decision variable $x_{i,t}$ is the load status in each time period, which is expressed as:

$$\min \sum_{i \in I} \sum_{t \in T} c_i x_{i,t} \tag{17}$$

where T is the set of time period.

The constraints of the restoration optimization are described as follows.

1) Steady Constraints and Load Constraints

The steady constraints and load constraints are similar to those in the load shedding optimization, which are omitted here.

2) DG Constraints

The output of dispatchable DG should not exceed its maximum, minimum, and ramp limits.

$$P_g^{\text{DDG,min}} \le P_{g,t,s}^{\text{DDG}} \le P_g^{\text{DDG,max}} \tag{18}$$

$$Q_g^{\text{DDG,min}} \le Q_{g,t,s}^{\text{DDG}} \le Q_g^{\text{DDG,max}} \tag{19}$$

$$\Delta P_g^{\text{dn,rs}} \le \Delta P_{g,t,s}^{\text{DDG}} - \Delta P_{g,t-1,s}^{\text{DDG}} \le \Delta P_g^{\text{up,rs}} \tag{20}$$

where $P_{g,t,s}^{\text{DDG}}$ and $Q_{g,t,s}^{\text{DDG}}$ are the active and reactive power of dispatchable DG g during period t in scenario s, respectively; $P_g^{\text{DDG,max}}$ and $P_g^{\text{DDG,min}}$ are the maximum and minimum active power of dispatchable DG g, respectively; $Q_g^{\text{DDG,max}}$ and $Q_g^{\text{DDG,min}}$ are the maximum and minimum reactive power of dispatchable DG g, respectively; and $\Delta P_g^{\text{up,rs}}$ and $\Delta P_g^{\text{dn,rs}}$ are the ramp-up and ramp-down power of dispatchable DG g during the restoration process, respectively.

The active power of RDG should be equal to the forecasting value, and the reactive power of RDG should not exceed its maximum and minimum limits.

$$P_{g,t,s}^{\text{RDG}} = P_{g,t,s}^{\text{RDG,sn}} \tag{21}$$

$$Q_g^{\text{RDG,min}} \le Q_{g,t,s}^{\text{RDG}} \le Q_g^{\text{RDG,max}} \tag{22}$$

where $P_{g,t,s}^{\text{RDG}}$ and $Q_{g,t,s}^{\text{RDG}}$ are the active and reactive power of RDG g during period t in scenario s, respectively; $P_{g,t,s}^{\text{RDG,sn}}$ is the forecasting active power of RDG g during period t in scenario s; and $Q_g^{\text{RDG,max}}$ and $Q_g^{\text{RDG,min}}$ are the maximum and minimum reactive power of RDG g, respectively.

All DGs should be within its rated capacity.

$$\left(P_{g,t,s}^{\text{DG}}\right)^2 + \left(Q_{g,t,s}^{\text{DG}}\right)^2 \le \left(S_g^{\text{DG}}\right)^2 \tag{23}$$

The reactive power of capacitor bank (CB) depends on its operation status.

$$Q_{c,t}^{\text{CB}} = z_{c,t} Q_c^{\text{CB,N}} \tag{24}$$

where $Q_{c,t}^{\text{CB}}$ is the reactive power of CB; $z_{c,t}$ is the operation status of CB, which is a binary variable, and $z_{c,t} = 1$ indicates that CB is in operation; and $Q_c^{\text{CB,N}}$ is the rated reactive power of CB.

3) Customer Comfort Constraint

In order to ensure the customer comfort, the number of status changes of each customer is limited to less than two times during the restoration process [30].

$$\sum_{t \in T} \left| x_{i,t} - x_{i,t-1} \right| \leq 2 \tag{25}$$

V. Simplification of Proposed Optimization Models

Due to the dynamic and nonlinear constraints as well as the binary-continuous variable, the proposed load shedding optimization and restoration optimization are complex. In this section, a simplified frequency response model and a linear power flow model are presented, which are used to linearize the above two optimization models into the MIQCP models.

A. Simplified Frequency Response Model

The maximum frequency deviation is the key index. In this paper, an approximate model of primary frequency response is used to calculate the maximum frequency deviation [46]. During the transition process, the ROCOF is calculated by the model of system frequency response as:

$$\mathrm{d}f/\mathrm{d}t = \Delta P/2H \tag{26}$$

where f is the system frequency; and H is the equivalent inertia.

Since the system power is balanced again after the transition, the initial power deficit $\Delta P(t_0)$ after load shedding is equal to the increased output of dispatchable DG during the transition process, which is formulated as:

$$\Delta P(t_0) = \sum_{g \in \Omega_{\mathrm{DDG}}} \left(P_g^{\mathrm{DDG}} - P_g^{\mathrm{DDG,bef}} \right) \tag{27}$$

where Ω_{DDG} is the set of dispatchable DG.

The governor of dispatchable DG responds to the frequency drop and increases the output. Therefore, the power deficit gradually decreases according to the ramp-up rate of DG R_g.

$$\Delta P(t) = \Delta P(t_0) - \sum_{g \in \Omega_{\mathrm{DDG}}} R_g (t - t_0) \tag{28}$$

When $\Delta P(t)$ is equal to 0 for the first time at $t = t_1$, the frequency deviation is the maximum (the stationary point). Therefore, the maximum frequency deviation during the transition process can be approximately calculated as:

$$\Delta f(t_1) = -\int_{t_0}^{t_1} \left\{ \frac{1}{2H} \left[\Delta P(t_0) - \sum_{g \in \Omega_{\mathrm{DDG}}} R_g (t - t_0) \right] \right\} \mathrm{d}t = \frac{1}{4H} \frac{\left[\sum_{g \in \Omega_{\mathrm{DDG}}} \left(P_g^{\mathrm{DDG}} - P_g^{\mathrm{DDG,bef}} \right) \right]^2}{\sum_{g \in \Omega_{\mathrm{DDG}}} R_g} \tag{29}$$

Figure 2 illustrates the process of governor adjustment and the change of frequency. It should be noted that the dependency of load on the voltage and frequency is ignored in this model. When the voltage and frequency are reduced during the transition process, the load demand will also be reduced, as shown in Fig. 2. As a result, this simplification leads to an optimistic estimate of the maximum frequency deviation $\left(\left| \Delta f(t_1') \right| < \left| \Delta f(t_1) \right| \right)$, which is conducive to make a conservative load shedding plan.

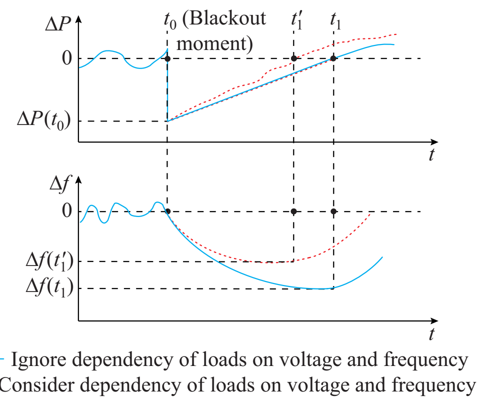

Fig. 2. Process of governor adjustment and change of frequency.

B. Linear Z-bus Power Flow Model

The linear power flow models have been widely used in optimization problems such as OPF. The widely-used linear DistFlow model [33] may lead to the unbalanced power because it ignores the network loss. Therefore, in this paper, the linear Z-bus power flow model is used [47], where the network loss is considered and S^{PCC} can be calculated analytically. The linear Z-bus power flow model is based on the fixed-point interpretation of the AC power flow equations, the process of which is as follows.

For the radial or meshed system with n nodes, firstly, the node voltages at the adjacent period (e.g., before the blackout) are regarded as the reference voltage $\boldsymbol{V}^{\mathrm{ref}} \in \mathbf{R}^{n \times 1}$. Then, the current power injections $\boldsymbol{X} = \left[\boldsymbol{P}^{\mathrm{T}} \quad \boldsymbol{Q}^{\mathrm{T}} \right]^{\mathrm{T}}$ are obtained through DMS, and the voltage $\boldsymbol{V} \in \mathbf{R}^{n \times 1}$, the voltage amplitude $|\boldsymbol{V}| \in \mathbf{R}^{n \times 1}$, the line current $\boldsymbol{I} \in \mathbf{R}^{l \times 1}$, and the power of PCC $S^{\mathrm{PCC}} \in \mathbf{R}^{1 \times 1}$ can be directly calculated as:

$$\boldsymbol{V} = \boldsymbol{M}\boldsymbol{X} + \boldsymbol{a} \tag{30}$$

$$|\boldsymbol{V}| = \boldsymbol{K}\boldsymbol{X} + \boldsymbol{b} \tag{31}$$

$$\boldsymbol{I} = \boldsymbol{J}\boldsymbol{X} + \boldsymbol{c} \tag{32}$$

$$S^{\mathrm{PCC}} = \boldsymbol{G}\boldsymbol{X} + d \tag{33}$$

where $\boldsymbol{M}$, $\boldsymbol{K}$, $\boldsymbol{J}$, $\boldsymbol{G}$, $\boldsymbol{a}$, $\boldsymbol{b}$, $\boldsymbol{c}$, and d are related to the reference voltage $\boldsymbol{V}^{\mathrm{ref}}$ as well as the admittance matrix $\boldsymbol{Y}$. More details can be found in [47].

The accuracy of the linear Z-bus power flow model depends on the difference between the current value and the reference value, and the accuracy can be improved by constantly updating the reference value with the solution value.

C. Simplification of Load Shedding Optimization

For the load shedding optimization, the dynamic constraint (4) and steady constraints (5)-(8) can be linearized through (29) and (30)-(33), respectively. For the load constraints (13) and (14), V_i^2 can be linearized around V_i^{ref} through Taylor series expansion as:

$$P_i = A_i^{\mathrm{P}} x_i V_i + B_i^{\mathrm{P}} x_i \tag{34}$$

where $A_i^{\mathrm{P}} = P_i^{\mathrm{N}}\left[\left(2V_i^{\mathrm{ref}}Z_i^{\mathrm{P}}\right)/\left(V_i^{\mathrm{N}}\right)^2 + I_i^{\mathrm{P}}/V_i^{\mathrm{N}}\right]$ and $B_i^{\mathrm{P}} = P_i^{\mathrm{N}}\left[P_i^{\mathrm{P}} - Z_i^{\mathrm{P}}/\left(V_i^{\mathrm{N}}V_i^{\mathrm{ref}}\right)^2\right]$.

Then, the binary-continuous variable x_iV_i can be linearized through the big-M method as:

$$\left(x_i-1\right)M \le V_i^{\mathrm{ax}} - V_i \le \left(1-x_i\right)M \tag{35}$$

$$-x_iM \le V_i^{\mathrm{ax}} \le x_iM \tag{36}$$

$$V_i^{\mathrm{ax}} = x_iV_i \tag{37}$$

where V_i^{ax} is the auxiliary binary variable; and M is a constant, which is set to be 1.5.

Then, the proposed load shedding optimization is formulated as an MIQCP model (the quadratic constraint is (12)), where the objective function is (1) and the constraints are (4)-(12), (15), and (29)-(37).

D. Simplification of Restoration Optimization

For the restoration optimization, the steady constraints and load constraints can be simplified similarly to those in the load shedding optimization. The constraint (25) can be linearized with the auxiliary binary variable $x_{i,t}^{\mathrm{ax}}$ in the following five inequality formulas.

$$x_{i,t}^{\mathrm{ax}} \le x_{i,t} + x_{i,t+1} \tag{38}$$

$$x_{i,t}^{\mathrm{ax}} \ge x_{i,t+1} - x_{i,t} \tag{39}$$

$$x_{i,t}^{\mathrm{ax}} \ge x_{i,t} - x_{i,t+1} \tag{40}$$

$$x_{i,t}^{\mathrm{ax}} \le 2 - x_{i,t} - x_{i,t+1} \tag{41}$$

$$\sum_{t\in T} x_{i,t}^{\mathrm{ax}} \le 2 \tag{42}$$

where $x_{i,t}^{\mathrm{ax}} = 1$ indicates that the status of load i changes during the period t.

Then, the proposed restoration optimization is formulated as an MIQCP model (the quadratic constraint is (23)), where the objective function is (17) and the constraints are (5)-(8), (18)-(24), and (30)-(42).

VI. Case Study

This section focuses on the simulation of the proposed load shedding strategy and restoration strategy. For the load shedding strategy, the effectiveness is firstly verified in Section VI-A. Then, by comparing with other research results, the importance of the correction table is proven in Section VI-B. For the restoration strategy, the effectiveness is firstly verified in Section VI-C. Then, the effectiveness of CVR in improving the restoration performance is compared in Section VI-D, and finally, the impact of the forecasting errors of PV output is analyzed in Section VI-E.

The modified IEEE 33-node system is employed as the simulation case, as shown in Fig. 3. The system has 32 loads, including municipal, industrial, commercial, and residential loads. The total number of customers is 460, and each load has a different number of customers. Municipal loads are the most important ones, followed by industrial and commercial loads, and finally the residential loads. The system has two dispatchable DGs (G1 and G2), three PVs (PV1, PV2, and PV3), and one CB. G2 is equipped with the wood-ward diesel governor (DEGOV1) and the simplified exciter system (SEX1) [30], which is the master DG during the intentional island operation, and other DGs are the salve ones. The status of the system is monitored by PMU in real time. For simplicity, the typical CVR factors are used to represent the effects of load CVR [40], as mentioned in Section IV. The optimization programs are solved by GUROBI 8.1.0, and the real-time digital simulation (RTDS) platform is used to simulate the transition process.

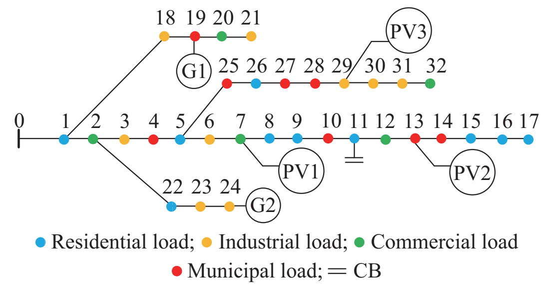

Fig. 3. Modified IEEE 33-node system.

A. Analysis of Proposed Load Shedding Strategy

The parameters of DG are shown in Table II. In the normal operation, the power supply of the main grid is 2410 kW, and the power supply of DGs is 1470 kW. Besides, the distribution system has a spinning reserve of 140 kW in G1 and G2. Therefore, in theory, the intentional island can restore up to 1610 kW loads during the transition process. The blackout is performed by disconnecting the circuit breaker at PCC.

TABLE II
Parameters of DG

Item	Node	P (kW)	Q (kvar)	S (kVA)	$\Delta P^{\mathrm{up,tr}}$ (kW)
PCC	0	2410	1204		
G1	19	200	150	600	30
G2	24	720	525	2400	110
PV1	7	180		545	
PV2	13	150		450	
PV3	29	220		660	
CB	11		500	500	

Before the grid is disconnected, the load shedding optimization proposed in Section III (LS1) is solved to obtain the optimal load shedding plan. According to the DG output, load demand, load priority, and the number of customers of loads, Table III lists the load shedding plans with LS1 and the load shedding strategy that only considers the priority factor (LS2) [15] , where the status of 1 indicates load shedding. It can be seen that there is a total of 18 loads that can be restored in LS1. The power of the restored load is 1605 kW, which is close to the maximum power of DG, indicating that the load shedding plan with LS1 makes full use of the DG resources.

Besides, with the help of the priority factor, it can be seen that the first-class loads are all restored with LS1, which is in line with the goal of intentional island, and the number of restored customers is 189. Due to the limited capacity of

DG, it is necessary to shed part of second-class loads to ensure the power balance.

TABLE III
LOAD SHEDDING PLANS WITH LS1 AND LS2

Load	Class	Power (kW)	Number of customers	Status	
				LS1	LS2
L_1	Third-class	100	10	1	1
L_2	Second-class	90	9	0	0
L_3	Second-class	120	10	0	0
L_4	First-class	60	7	0	0
L_5	Third-class	60	5	1	1
L_6	Second-class	200	24	1	1
L_7	Second-class	200	28	1	1
L_8	Second-class	60	3	0	0
L_9	Third-class	60	7	1	1
L_{10}	First-class	45	4	0	0
L_{11}	Third-class	60	6	1	1
L_{12}	Second-class	60	7	0	0
L_{13}	First-class	120	18	0	0
L_{14}	First-class	60	10	0	0
L_{15}	Third-class	60	4	1	1
L_{16}	Third-class	60	12	0	1
L_{17}	Third-class	90	18	1	1
L_{18}	Second-class	90	16	0	0
L_{19}	First-class	90	20	0	0
L_{20}	Second-class	90	10	0	0
L_{21}	Second-class	90	6	1	0
L_{22}	Third-class	90	8	1	1
L_{23}	Second-class	420	60	1	1
L_{24}	Second-class	420	70	1	1
L_{25}	First-class	60	6	0	0
L_{26}	Third-class	60	6	1	0
L_{27}	First-class	60	6	0	0
L_{28}	First-class	120	11	0	0
L_{29}	Second-class	200	19	1	0
L_{30}	Second-class	150	14	0	1
L_{31}	Second-class	210	20	0	1
L_{32}	Second-class	60	6	0	0

The load shedding plan with LS2 is also calculated to verify the necessity of the proposed customer factor in load weight. As shown in Table III, the number of restored loads with LS2 is 18, which equals that with LS1. However, the power of the restored load with LS2 is 1535 kW and the number of restored customers is 174, which are significantly lower than those with LS1, and this is because LS2 randomly selects the load with same priority. For example, LS2 sheds L_{16} with more customers instead of L_{26} with fewer customers, which is disadvantageous to the SAIDI. In contrast, LS1 considers more factors in the load weight such as the number of customers. Therefore, the load shedding plan is more reasonable and the load shedding cost is lower. For example, L_2, L_{18}, L_{20}, and L_{21} are all second-class loads with the same power demand, and LS1 chooses L_{21} that has the least number of customers to be shed. With the help of customer factor, LS1 automatically selects the load with a small number of customers to be shed, which is favorable to the SAIDI.

Different from the conventional RLS strategy (LS3) driven by the frequency change, LS1 is driven by the status of the circuit breaker at PCC (i.e., the blackout event). When the blackout occurs, the system frequencies during the transition process with LS1 and LS3 [8] are shown in Fig. 4. It can be seen that the frequency with LS3 has considerably higher undershoot and overshoot compared with LS1. The corresponding key indices during the transition process with LS1 and LS3 are shown in Table IV, where f^{max} and f^{min} are the maximum and minimum frequencies, respectively; and V^{max} and V^{min} are the maximum and minimum node voltages, respectively. It can be seen that the deviations of frequency and voltage with LS1 are smaller than those with LS3.

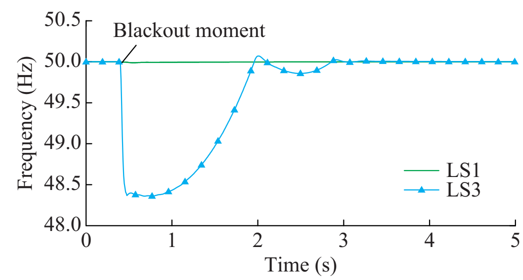

Fig. 4. System frequencies during transition process with LS1 and LS3.

TABLE IV
KEY INDICES DURING TRANSITION PROCESS WITH LS1 AND LS3

Strategy	f^{max} (Hz)	f^{min} (Hz)	V^{max} (p.u.)	V^{min} (p.u.)
LS1	50.01	49.92	1.01	0.98
LS3	50.07	48.34	1.08	0.85

B. Effectiveness of Correction Table in Load Shedding

The correction table is generated according to the load shedding plan, as shown in Table V. For simplification, only part of the correction table is listed. It can be seen that for $60\ \text{kW} \leq \Delta P^{PCC} < 165\ \text{kW}$, the third-class load L_9 with the largest number of customers is selected to be preferentially restored. The reason why the second-class loads are not selected is that the power of each second-class load (L_6, L_7, L_{21}, L_{23}, L_{24}, and L_{29}) is larger than 60 kW, which exceeds the lower limit of the power interval. For $-45\ \text{kW} \leq \Delta P^{PCC} < 0$, L_{16} with the lowest priority is selected to be preferentially shed. The results of the correction table are in line with the principles of correction table in Section III.

Assuming that the fluctuation of PV is rapid, and the total power of PV reduces to 508 kW and the ΔP^{PCC} is -42 kW at the moment of blackout. Therefore, L_{16} is additionally shed according to the correction table. The system frequencies during the transition process with LS1 and the strategy without correction table (LS4) [19] are compared, as shown in Fig. 5. The corresponding key indices during the transition process with LS1 and LS4 are shown in Table VI. Due to the rapid fluctuation of PV, the previously calculated load shedding plan is not suitable for the current system. Therefore, there is a mismatch between the DG output and the restored load demand with LS4. Compared with LS1, the frequency with LS4 has higher undershoot and overshoot. On the contrary, by using real-time PMU data, LS1 online corrects the load shedding plan through the correction table, which ensures the power balance and smooth transition of the intentional island. It can be seen from Fig. 5 that LS1 has no frequency overshoot, indicating that the load shedding is valid when the fluctuation of PV is rapid.

TABLE V
CORRECTION TABLE WITH LS1

Scenario	Power interval	Results of load shedding correction
⋮	⋮	⋮
S_i	$165\ \text{kW} \le \Delta P^{\text{PCC}} < 270\ \text{kW}$	Additionally restore L_9, L_{21}
S_{i+1}	$60\ \text{kW} \le \Delta P^{\text{PCC}} < 165\ \text{kW}$	Additionally restore L_9
S_{i+2}	$0\ \text{kW} \le \Delta P^{\text{PCC}} < 60\ \text{kW}$	
S_{i+3}	$-45\ \text{kW} \le \Delta P^{\text{PCC}} < 0\ \text{kW}$	Additionally shed L_{16}
S_{i+4}	$-125\ \text{kW} \le \Delta P^{\text{PCC}} < -45\ \text{kW}$	Additionally shed L_2, L_{16}
⋮	⋮	⋮

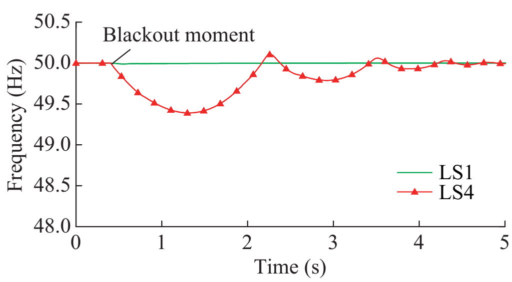

Fig. 5. System frequencies during transition process with LS1 and LS4.

TABLE VI
KEY INDICES DURING TRANSITION PROCESS WITH LS1 AND LS4

Strategy	$f^{\max}$ (Hz)	$f^{\min}$ (Hz)	$V^{\max}$(p.u.)	$V^{\min}$(p.u.)
LS1	50.03	49.94	1.01	0.99
LS4	50.11	49.39	1.03	0.92

C. Analysis of Restoration Strategy

Assuming that the blackout duration is 1 hour and each time period is set to be 15 min. The demand of each load and the output of each PV follow the same profile during the restoration process. Figure 6 lists the multipliers of load demand and PV output in 10 dynamic scenarios (S_1-S_{10}) as well as measurement and forecasting values of PV output during each period (T_1-T_4).

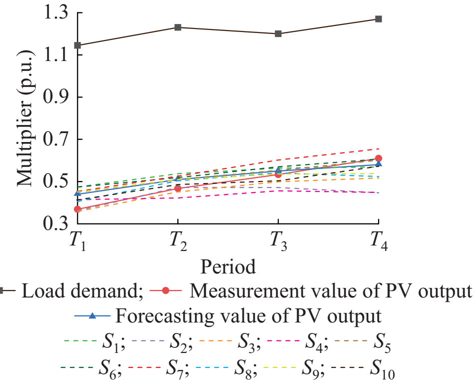

Fig. 6. Multipliers of load demand and PV output.

The multi-period restoration plan obtained with the proposed restoration strategy (RS1) is shown in Table VII. By increasing the outputs of G1 and G2, the number of restored loads during T_1 reaches 27, which is much larger than that during the transition process. Besides, the first-class loads are all restored during all periods, which is consistent with the goal of the intentional island. Meanwhile, according to the changes of load demand and PV output, the restoration plan is adjusted automatically to optimize the restoration performance while maintaining the power balance. For example, the load demand increases from 4068 kW during T_1 to 4384 kW during T_2, which exceeds the increase of PV output. Therefore, the number of restored loads is reduced during T_2 to ensure the power balance. In addition, during T_3, the number of the restored loads increases because the PV output increases but load demand decreases. To sum up, with the help of the RS1, the DG resources are optimally distributed during each period with the optimal restoration performance.

D. Effectiveness of CVR in Improving Restoration Performance

In order to verify the effectiveness of CVR in improving the restoration performance, RS1 is compared with the restoration strategy without CVR (RS2) [26]. The accumulation of restored loads with RS1 and RS2 is shown in Table VII. It can be seen that the restoration performance with RS1 is better than that with RS2 during all periods. In addition, since CVR reduces the load demand and the granularity of load demand, the load combination that is more suitable for DG output can be found. Therefore, the restored load with RS1 is higher than that with RS2. Moreover, taking T_1 as an example, when the DG output reaches its limit, the number of restored loads can be further increased from 22 to 27 by reducing the power of each customer through CVR.

TABLE VII
MULTI-PERIOD RESTORATION PLAN WITH RS1

Period	Load demand (kW)	Restored load (kW)	Number of restored loads	Number of restored customers	Total DG output (kW)	Restoration rate of the first-class load (%)
T_1	4068	3120	27	348	3208	100
T_2	4384	3220	23	332	3303	100
T_3	4272	3283	27	347	3369	100
T_4	4532	3256	22	323	3339	100

TABLE VII
ACCUMULATION OF RESTORED LOADS WITH RS1 AND RS2

Period	Strategy	Restored loads (kW)	Number of restored loads	Number of restored customers
T_1	RS1	3120	27	348
	RS2	2907	22	313
T_2	RS1	3220	23	332
	RS2	3201	22	323
T_3	RS1	3283	27	347
	RS2	3120	22	313
T_4	RS1	3256	22	323
	RS2	3059	21	293

However, it should be noted that CVR should be implemented on the premise that the node voltage is within the statutory limit. The node voltages with RS1 and RS2 during each period are shown in Fig. 7. It can be seen that there are two different sets of voltage curves. The node voltages with RS2 are around 1.0 p.u., while those with RS1 are close to 0.9 p.u.. Although the node voltages with RS1 are lower than those with RS2, they are within the limit with little impact on customers. Therefore, although CVR is limited by the load type and voltage, the above results clearly show that CVR can restore more loads, which provides a new method for system operators to improve the restoration performance.

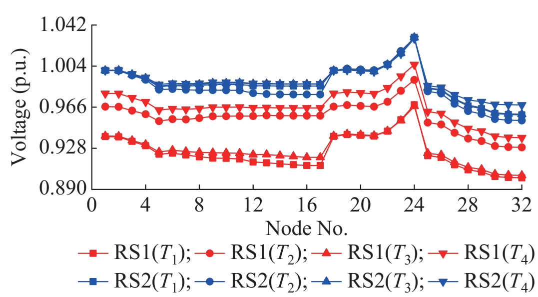

Fig. 7. Node voltages with RS1 and RS2 during each period.

E. Impact of Forecasting Error of PV Output on Restoration

In this subsection, RS1 is compared with the restoration strategy using the forecasting values of PV output (RS3) [30]. It can be seen from Fig. 6 that the forecasting values of PV output during T_1, T_2, and T_3 are higher than the actual output. As a result, RS3 will restore more loads based on the forecasting values of PV. The total power demands with RS1 and RS3 (including the load demand and the network loss) and the actual range of DG output are shown in Fig. 8. It can be seen that the load demand with RS3 exceeds the maximum DG output during T_1, T_2, and T_3, which may threaten the system operation. In contrast, since the forecasting error is taken into account in the dynamic scenario, RS1 is robust to the PV uncertainty, which ensures that the load demand is always within the range of DG output. Therefore, it is necessary to consider the forecasting errors of PV output in order to maintain the stable operation of the intentional island.

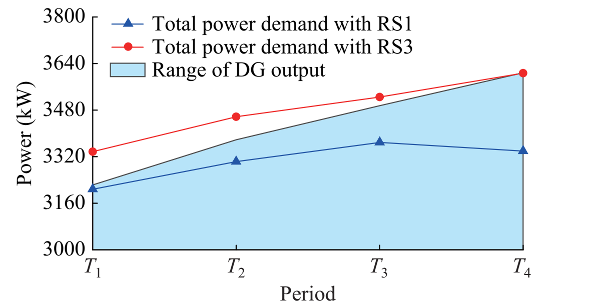

Fig. 8. Total power demands with RS1 and RS3 and actual range of DG output.

VII. CONCLUSION

This paper proposes a PMU-based load shedding strategy and a CVR-based multi-period restoration strategy. Through the combination of load shedding optimization and correction table, the power mismatch caused by the real-time power fluctuation of RDG during the load shedding process is minimized, so that the intentional island can be seamlessly transitioned with the optimal load curtailment. Besides, the multi-period restoration plans are generated, which can effectively ensure the power balance under the drastic intermittence of PV output on a long time scale. Meanwhile, CVR is also implemented to improve the restoration performance. In order to verify the effectiveness of the proposed strategies, this paper takes the IEEE 33-node system as the simulation case, and the results are concluded as follows.

1) The proposed event-based load shedding strategy can perform the optimal load shedding immediately, which has better transient characteristics than the conventional response-based strategy.

2) Establishing the correction table helps make the effective load shedding plan online, which reduces the impact of real-time fluctuation of PV.

3) During the restoration process, more customers can be restored by reasonably reducing the load demand based on CVR.

4) By representing the forecasting values of PV output by dynamic scenarios, the robustness of the restoration plan is improved.

The future work will focus on the utilization of existing equipment as well as the consideration of time-varying CVR effects.

REFERENCES

[1] H. Qi, X. Wang, L. Tolbert *et al*., "A resilient real-time system design for a secure and reconfigurable power grid," *IEEE Transactions on Smart Grid*, vol. 2, no. 4, pp. 770-781, Dec. 2011.

[2] National Energy Administration of China. (2016, Nov). Five-year power development plan (2016-2020). [Online]. Available: http://fjb.nea.gov.cn/news_view.aspx?id=27538

[3] C. Huang, F. Li, D. Zhou *et al*., "Data quality issues for synchrophasor applications Part I: a review," *Journal of Modern Power Systems and Clean Energy*, vol. 4, no. 2, pp. 342-252, Jul. 2016.

[4] M. H. Oboudi, M. Mohammadi, and M. Rastegar, "Resilience-oriented intentional islanding of reconfigurable distribution power systems," *Journal of Modern Power Systems and Clean Energy*, vol. 7, no. 4, pp. 741-752, Jul. 2019.

[5] *IEEE Application Guide for IEEE STD 1547, IEEE Standard for Interconnected Distributed Resources with Electric Power Systems*, IEEE

Standard 1547.2-2008, 2009.

[6] K. Das, F. Guo, E. Nuño *et al*., "Frequency stability of power system with large share of wind power under storm conditions," *Journal of Modern Power Systems and Clean Energy*, vol. 8, no. 2, pp. 219-228, Mar. 2020.

[7] L. Sigrist, I. Egido, and L. Rouco, "A method for the design of UFLS schemes of small isolated power systems," *IEEE Transactions on Power Systems*, vol. 27, no. 2, pp. 951-958, May 2012.

[8] A. Ketabi and M. F. Hajiakbari, "An underfrequency load shedding scheme for islanded microgrids," *International Journal of Electrical Power & Energy Systems*, vol. 62, pp. 599-607, Nov. 2014.

[9] M. Karimi, P. Wall, H. Mokhlis *et al*., "A new centralized adaptive underfrequency load shedding controller for microgrids based on a distribution state estimator," *IEEE Transactions on Power Delivery*, vol. 32, no. 1, pp. 370-380, Feb. 2017.

[10] B. de Nadai Nascimento, A. C. Z. de Souza, J. G. de Carvalho Costa *et al*., "Load shedding scheme with under-frequency and undervoltage corrective actions to supply high priority loads in islanded microgrids," *IET Renewable Power Generation*, vol. 13, no. 11, pp. 1981-1989, Aug. 2019.

[11] F. Zare, A. Ranjbar, and F. Faghihi, "Intelligent topology-oriented LS scheme in power systems integrated with high wind power penetration," *IET Generation*, *Transmission & Distribution*, vol. 14, no. 9, pp. 1684-1693, Apr. 2020.

[12] B. Delfino, S. Massucco, A. Morini *et al*., "Implementation and comparison of different under frequency load-shedding schemes," in *Proceedings of 2001 PES Summer Meeting*, Vancouver, Canada, Feb. 2001, pp. 307-312.

[13] Y. Zuo, G. Frigo, A. Derviškadić *et al*., "Impact of synchrophasor estimation algorithms in ROCOF-based under-frequency load-shedding," *IEEE Transactions on Power Systems*, vol. 35, no. 2, pp. 1305-1316, Mar. 2020.

[14] Q. Zhou, Z. Li, Q. Wu *et al*., "Two-stage load shedding for secondary control in hierarchical operation of islanded microgrids," *IEEE Transactions on Smart Grid*, vol. 10, no. 3, pp. 3103-3111, May 2019.

[15] T. Shekari, A. Gholami, F. Aminifar *et al*., "An adaptive wide-area load shedding scheme incorporating power system real-time limitations," *IEEE Systems Journal*, vol. 12, no. 1, pp. 759-767, Mar. 2018.

[16] H. Yuan and Y. Xu, "Preventive-corrective coordinated transient stability dispatch of power systems with uncertain wind power," *IEEE Transactions on Power Systems*, vol. 35, no. 5, pp. 3616-3626, Sept. 2020.

[17] M. Gautam, N. Bhusal, and M. Benidris, "A sensitivity-based approach to adaptive under-frequency load shedding," in *Proceedings of 2020 IEEE Texas Power and Energy Conference (TPEC)*, College Station, USA, Feb. 2020, pp. 1-5.

[18] H. Gao, Y. Chen, Y. Xu *et al*., "Dynamic load shedding for an islanded microgrid with limited generation resources," *IET Generation*, *Transmission & Distribution*, vol. 10, no. 12, pp. 2953-2961, Aug. 2016.

[19] G. Liu, B. Xiao, and M. Starke, "A robust load shedding strategy for microgrid islanding transition," in *Proceedings of 2016 IEEE/PES Transmission and Distribution Conference and Exposition (T&D)*, Dallas, USA, May 2016, pp. 1-5.

[20] Y. Fan, X. Zi, L. Jun *et al*., "Research on optimal load shedding for active distribution network based on genetic algorithm," in *Proceedings of 2017 2nd International Conference on Power and Renewable Energy (ICPRE)*, Chengdu, China, Sept. 2017, pp. 510-514.

[21] Y. Hong and M. Nguyen, "Multiobjective multiscenario under-frequency load shedding in a standalone power system," *IEEE Systems Journal*, vol. 14, no. 2, pp. 2759-2769, Jun. 2020.

[22] M. Gholami, J. Moshtagh, and N. Ghadernejad, "Service restoration in distribution networks using combination of two heuristic methods considering load shedding," *Journal of Modern Power Systems and Clean Energy*, vol. 3, no. 4, pp. 556-564, Dec. 2015.

[23] A. Hussain, V. Bui, and H. Kim, "An effort-based reward approach for allocating load shedding amount in networked microgrids using multiagent system," *IEEE Transactions on Industrial Informatics*, vol. 16, no. 4, pp. 2268-2279, Apr. 2020.

[24] I. de la Parra, J. Marcos, and M. Garcia, "Control strategies to use the minimum energy storage requirement for PV power ramp-rate control," *Solar Energy*, vol. 111, pp. 332-343, Jan. 2015.

[25] F. Shen, Q. Wu, and Y. Xue, "Review of service restoration for distribution networks," *Journal of Modern Power Systems and Clean Energy*, vol. 8, no. 1, pp. 1-14, Jan. 2020.

[26] J. Li, X. Ma, C. Liu *et al*., "Distribution system restoration with microgrids using spanning tree search," *IEEE Transactions on Power Systems*, vol. 29, no. 6, pp. 3021-3029, Nov. 2014.

[27] D. Feng, F. Wu, Y. Zhou *et al*., "Multi-agent-based rolling optimization method for restoration scheduling of distribution systems with distributed generation," *Journal of Modern Power Systems and Clean Energy*, vol. 8, no. 4, pp. 737-749, Jul. 2020.

[28] Y. Liu, R. Fan, and V. Terzija, "Power system restoration: a literature review from 2006 to 2016," *Journal of Modern Power Systems and Clean Energy*, vol. 4, no. 3, pp. 332-341, Jul. 2016.

[29] V. Hosseinnezhad, M. Rafiee, M. Ahmadian *et al*., "Optimal island partitioning of smart distribution systems to improve system restoration under emergency conditions," *International Journal of Electrical Power & Energy Systems*, vol. 97, pp. 155-164, Apr. 2018.

[30] Y. Xu, C. Liu, Z. Wang *et al*., "DGs for service restoration to critical loads in a secondary network," *IEEE Transactions on Smart Grid*, vol. 10, no. 1, pp. 435-447, Jan. 2019.

[31] S. Ghasemi, A. Khodabakhshian, and R. Hooshmand, "New multi-stage restoration method for distribution networks with DGs," *IET Generation*, *Transmission & Distribution*, vol. 13, no. 1, pp. 55-63, Jan. 2019.

[32] H. Sekhavatmanesh and R. Cherkaoui, "A novel decomposition solution approach for the restoration problem in distribution networks," *IEEE Transactions on Power Systems*, vol. 35, no. 5, pp. 3810-3824, Sept. 2020.

[33] B. Chen, C. Chen, J. Wang *et al*., "Multi-time step service restoration for advanced distribution systems and microgrids," *IEEE Transactions on Smart Grid*, vol. 9, no. 6, pp. 6793-6805, Nov. 2018.

[34] A. Abessi and S. Jadid, "Internal combustion engine as a new source for enhancing distribution system resilience," *Journal of Modern Power Systems and Clean Energy*, doi: 10.35833/MPCE.2019.000246.

[35] J. Zhao, M. Zhang, H. Yu *et al*., "An islanding partition method of active distribution networks based on chance-constrained programming," *Applied Energy*, vol. 242, no. 6, pp. 78-91, May 2019.

[36] G. Huang, J. Wang, C. Chen *et al*., "Integration of preventive and emergency responses for power grid resilience enhancement," *IEEE Transactions on Power Systems*, vol. 32, no. 6, pp. 4451-4463, Nov. 2017.

[37] Z. Wang and J. Wang, "Service restoration based on AMI and networked MGs under extreme weather events," *IET Generation*, *Transmission & Distribution*, vol. 11, no. 2, pp. 401-408, Jan. 2017.

[38] C. Wang, S. Lei, P. Ju *et al*., "MDP-based distribution network reconfiguration with renewable distributed generation: approximate dynamic programming approach," *IEEE Transactions on Smart Grid*, vol. 11, no. 4, pp. 3620-3631, Jul. 2020.

[39] M. Waseem, Z. Lin, Y. Ding *et al*., "Technologies and practical implementations of air-conditioner based demand response," *Journal of Modern Power Systems and Clean Energy*, doi: 10.35833/MPCE.2019.000449.

[40] Z. Wang and J. Wang, "Review on implementation and assessment of conservation voltage reduction," *IEEE Transactions on Power Systems*, vol. 29, no. 3, pp. 1306-1315, May 2014.

[41] R. Jamalzadeh and M. Hong, "Microgrid optimal power flow using the generalized benders decomposition approach," *IEEE Transactions on Sustainable Energy*, vol. 10, no. 4, pp. 2050-2064, Oct. 2019.

[42] M. S. Hossan and B. Chowdhury, "Integrated CVR and demand response framework for advanced distribution management systems," *IEEE Transactions on Sustainable Energy*, vol. 11, no. 1, pp. 534-544, Jan. 2020.

[43] *Technical Requirements for the Design of Power Supply and Distribution System*, Chinese National Standard GB 50052-2009, 2009.

[44] *IEEE Guide for Electric Power Distribution Reliability Indices*, IEEE Standard 1366-2012, 2012.

[45] J. Xu, J. Wang, S. Liao *et al*., "Stochastic multi-objective optimization of photovoltaics integrated three-phase distribution network based ondynamic scenarios," *Applied Energy*, vol. 231, pp. 985-996, Dec. 2018.

[46] Y. Zhou, W. Hu, Y. Min *et al*., "Active splitting strategy searching approach based on MISOCP with consideration of power island stability," *Journal of Modern Power Systems and Clean Energy*, vol. 7, no. 3, pp. 475-490, May 2019.

[47] A. Bernstein, C. Wang, E Dall'Anese *et al*., "Load-flow in multiphase distribution networks: existence, uniqueness, and linear models," *IEEE Transactions on Power Systems*, vol. 33, no. 6, pp. 5832-5843, Nov. 2018.

Jian Xu received the B.S. and Ph.D. degrees in electrical engineering from Wuhan University, Wuhan, China, in 2002 and 2007, respectively. He is currently a Professor with the School of Electrical Engineering and Automation, Wuhan University. His research interests include power system opera-

tion, voltage stability, and wind power control and integration.

Boyu Xie received the B.S. degree in electrical engineering from Wuhan University, Wuhan, China, in 2017. He is currently working toward the Ph.D. degree in the School of Electrical Engineering and Automation, Wuhan University. His research interests include distribution system operation, renewable energy, and load control.

Siyang Liao received the B.S. and Ph.D. degrees in electrical engineering from Wuhan University, Wuhan, China, in 2011 and 2016, respectively. He is currently an Associated Professor with the School of Electrical Engineering and Automation, Wuhan University. His research interests include wind power integration and power system simulation.

Zhiyong Yuan received the Ph.D. degree in electrical engineering from Tsinghua University, Beijing, China, in 2006. He is currently the Director of the Distribution Department, Electric Power Research Institute, China Southern Power Grid Company, Guangzhou, China. His research interests include synchronous smart distribution networks and intelligent sensor.

Deping Ke received the B.S. degree in electrical engineering from the Huazhong University of Science and Technology, Wuhan, China, in 2005, and the Ph.D. degree in electrical engineering from Hong Kong Polytechnic University, Hong Kong, in 2012. He is currently an Associate Professor with the School of Electrical Engineering and Automation, Wuhan University, Wuhan, China. His research interests include power system dynamics and control, and economical operation of power systems.

Yuanzhang Sun received the Ph.D. degree in electrical engineering from Tsinghua University, Beijing, China, in 1988. He is currently a Professor with the School of Electrical Engineering and Automation, Wuhan University, Wuhan, China, and a Chair Professor with the Department of Electrical Engineering and Vice Director of the State Key Laboratory of Power System Control and Simulation, Tsinghua University. His research interests include power system dynamics and control, voltage stability and control, and reliability.

Xiong Li received the Ph.D. degree from Tsinghua University, Beijing, China, in 1997. He is an Associate Professor with Wuhan University, Wuhan, China. His main research interest is power system control based on wide area measurement system (WAMS).

Xiaotao Peng received the B.S. degree in control engineering, and the M.S. and Ph.D. degrees in electrical engineering from Huazhong University of Science and Technology, Wuhan, China, in 1993, 2002, and 2006, respectively. He is currently an Associate Professor with the School of Electrical Engineering and Automation, Wuhan University, Wuhan, China. His research interests include power system stability analysis and control, renewable energy, high-voltage direct current (HVDC), and application of energy storage system.